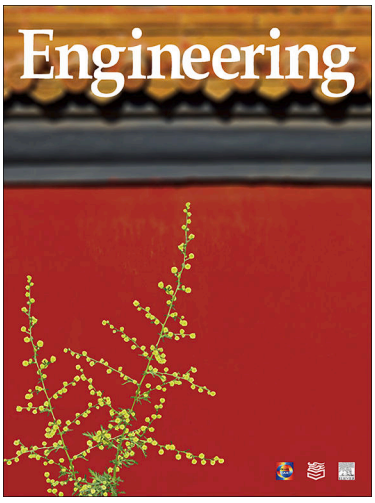
Journal Pre-proofs



Article

Diffusion Strategy of Water Electrolytic Hydrogen in Desert Energy Systems and Ecosystems

Jiarong Li, Zifu Zhang, Jiaxin Xu, Jin Lin, Huimin Lei, Mun S. Ho, Chris P. Nielsen, Jianxiao Wang, Feng Song, Xinxin Pang, Yonghua Song, Michael B. McElroy

PII: S2095-8099(26)00572-2
DOI: https://doi.org/10.1016/j.eng.2026.09.015
Reference: ENG 2486

To appear in: *Engineering*

Received Date: 27 November 2025
Revised Date: 18 August 2026
Accepted Date: 24 September 2026

Please cite this article as: J. Li, Z. Zhang, J. Xu, J. Lin, H. Lei, M.S. Ho, C.P. Nielsen, J. Wang, F. Song, X. Pang, Y. Song, M.B. McElroy, Diffusion Strategy of Water Electrolytic Hydrogen in Desert Energy Systems and Ecosystems, *Engineering* (2026), doi: https://doi.org/10.1016/j.eng.2026.09.015

This is a PDF of an article that has undergone enhancements after acceptance, such as the addition of a cover page and metadata, and formatting for readability. This version will undergo additional copyediting, typesetting and review before it is published in its final form. As such, this version is no longer the Accepted Manuscript, but it is not yet the definitive Version of Record; we are providing this early version to give early visibility of the article. Please note that Elsevier's sharing policy for the Published Journal Article applies to this version, see: https://www.elsevier.com/about/policies-and-standards/sharing#4-published-journal-article. Please also note that, during the production process, errors may be discovered which could affect the content, and all legal disclaimers that apply to the journal pertain.

© 2026 THE AUTHORS. Published by Elsevier LTD on behalf of Chinese Academy of Engineering and Higher Education Press Limited Company

Research

Environmental Frontiers for Water–Energy Nexus—Article

Diffusion Strategy of Water Electrolytic Hydrogen in Desert Energy Systems and Ecosystems

Jiarong Li[a,#], Zifu Zhang[b,#], Jiaxin Xu[c], Jin Lin[c,d,*], Huimin Lei[b,*], Mun S. Ho[a], Chris P. Nielsen[a], Jianxiao Wang[e,*], Feng Song[f], Xinxin Pang[g], Yonghua Song[h], Michael B. McElroy[a,*]

[a]*Harvard John A. Paulson School of Engineering and Applied Sciences, Harvard University, Cambridge, Massachusetts, 02138, USA.*

[b]*School of Civil Engineering, Tsinghua University, Beijing, 100084, China.*

[c]*Department of Electrical Engineering, Tsinghua University, Beijing, 100084, China.*

[d]*State Key Laboratory of Power System Operation and Control, Tsinghua University, Beijing, 100084, China.*

[e]*National Engineering Laboratory for Big Data Analysis and Applications, Peking University, Beijing, 100871, China.*

[f]*School of Applied Economics, Renmin University of China, Beijing, 100872, China.*

[g]*China Electric Power Planning and Engineering Institute, Beijing, 100120, China.*

[h]*State Key Laboratory of Internet of Things for Smart City, University of Macau, Macau, 999078, China.*

[#]The authors contribute equally.

*Correspondence authors
E-mail addresses: linjin@tsinghua.edu.cn (J. Lin), leihm@mail.tsinghua.edu.cn (H. Lei), wang-jx@pku.edu.cn (J. Wang), mbm@seas.harvard.edu (M. McElroy).

Abstract

Deploying photovoltaic (PV) systems in desert regions can support both decarbonization and ecological restoration, but conventional photovoltaic-to-grid (PVtG) strategies face increasing integration costs, curtailment, and value deflation as deployment scales up. This study proposes a novel water–energy–ecology coupling mode for desert PV development by integrating PVtG with onsite photovoltaic-to-hydrogen (PVtH) systems through segmented temporal partitioning. To evaluate this nexus, we develop a nonlinear multiscale framework that enables consistent evaluation of how local PV deployment decisions translate into system-wide decarbonization, financial cost, and biomass outcomes. Using the Kubuqi Desert—the seventh largest desert in China—as a testbed, we identify the scaling law of PV utilization by evaluating eight temporal partition strategies across PV capacities up to 25 gigawatts (GW). The results show that pure PVtG strategies exhibit diseconomies of scale, increasing unit cost by 1.6×10^{-3} USD • (kW • h)$^{-1}$. In contrast, hybrid strategies that allocate peak generation to PVtH reduce system costs by up to 1.0×10^{-3} USD • (kW • h)$^{-1}$. The cost-efficient 25 GW strategy annually withdraws 25.25 million tonnes (Mt) of water, delivers 25.30 TW • h of electricity, and produces 0.36 Mt of green hydrogen. This strategy achieves a 24 Mt reduction in CO_2 emissions and a 4×10^4 t increase in biomass. This hybrid approach outperforms alternatives such as carbon capture and grass pads, with total cost savings of 0.90 billion USD. Sensitivity analysis further reveals that water availability and grid-side storage strongly affect the optimal partition trajectory, while carbon prices of 12.86–15.43 USD • tCO_2^{-1} can close the financial gap without subsidies. To support implementation, water and land regulations and segmented power purchase agreements (PPAs) are recommended.

Keywords: Desert ecosystem restoration, Carbon abatement, Photovoltaic-to-hydrogen (PVtH), Spatiotemporal partitioning strategy

1 Introduction

In the 21st century, climate change and desertification have made reducing carbon emissions and restoring desert ecosystems urgent tasks, aligning with the United Nations Sustainable Development Goals (SDGs 13 and 15) [1]. Deploying photovoltaic (PV) panels in deserts has attracted global attention in recent years [2–3]. Specifically, PV panels can increase vegetation growth by stabilizing soil and altering microclimatic conditions: shading from PV panels reduces surface evaporation and lowers soil temperature, thereby preserving soil moisture and promoting increases in biomass (defined below, representing the ecological value discussed in this research) [4–9]. Moreover, clean solar energy contributes to the decarbonization of fossil fuel-based sectors. Recognizing these dual ecological and energy benefits, China's National Development and Reform Commission proposed

constructing 455 gigawatts (GW) of PV and wind capacity in its desert, gobi, and barren areas by 2030 [10]. Early evidence from completed projects, including 2 GW installed in the Kubuqi Desert by 2024 [11], demonstrates significant ecological improvements, validating the potential for large-scale PV deployment to combat desertification.

Currently, large-scale desert PV deployment primarily adopts the photovoltaic-to-grid (PVtG) approach, which connects PV-generated electricity to power grids via remote substations and transmission lines. However, this approach faces substantial challenges that limit the economic–environmental performance of PV investments. First, remote PV generation is associated with high transmission costs and accessibility barriers, significantly increasing the costs of meeting ecological goals. Second, owing to the intermittent nature of solar energy, maintaining grid stability requires costly energy storage and complex power-balancing solutions [12–13]. Moreover, the concentration of PV generation around midday causes notable market value deflation, reducing prices and economic returns [14]. These technical and economic challenges limit the commercial viability of using PVtG for decarbonization and ecological improvement.

To increase the cost-effectiveness of PV systems, we propose the use of onsite PVtH systems, which directly convert PV electricity to green hydrogen through water electrolyzers deployed at desert PV locations. The green hydrogen produced onsite can effectively decarbonize fossil fuel-dependent sectors traditionally, such as those involving chemical production, steelmaking, and transportation [15–18]. Moreover, reusing cooling water from electrolyzer systems for onsite irrigation can further benefit the ecosystem beneath PV panels. PVtH can strategically complement PVtG by optimally allocating daily generation to the grid or to hydrogen production using customized power purchase agreements (PPAs) [19–20]. By using segmented daily utilization profiles, compared with PVtG alone, PVtG–PVtH strategies more efficiently channel solar radiation and water resources into carbon reduction and ecological values.

However, two important questions remain insufficiently addressed in the literature. First, although previous studies have separately shown that PV deployment can generate ecological benefits and that PVtH can improve the value of solar electricity, the integrated water–energy–ecology coupling mode remains unclear, particularly in terms of how water availability and use interact with the dual pathways of grid export and hydrogen production to affect ecological restoration outcomes. Second, existing studies have focused mainly on the performance of specific strategies at a single deployment scale, whereas the sustainability pathway and scale effects associated with PV expansion remain underexplored. Addressing these questions requires a framework that can jointly characterize water and PV utilization, represent the ecological effects induced by PV deployment and water use, and propagate these coupled effects to system-level outcomes.

Methodologically, the literature has approached the problem from three largely separate directions. With respect to PVtG deployment, previous studies have relied mainly on power system operation, dispatch, and grid integration assessments to quantify the balancing requirements, storage needs, transmission costs, and market value deflation associated with large-scale solar integration. With respect to PV ecology, recent studies have adopted a diverse set of methods to identify environmental responses to PV deployment. A global meta-analysis synthesized 42 original studies to quantify changes in wind speed, soil temperature, soil moisture, and gross primary productivity around PV plants [21]. Field monitoring in a warm-desert ecovoltaic system revealed how panel layout and precipitation timing reshape local radiation, evaporative demand, soil temperature, and soil moisture patterns [22]. In Inner Mongolia, a recent study applied double machine learning to estimate the causal effects of PV installations on grassland productivity and highlighted strong spatial heterogeneity in ecological responses [23], whereas a national-scale assessment evaluated the sustainability co-benefits of PV deployment on suitable marginal land [24]. With respect to PVtH, existing studies have focused mainly on hydrogen-oriented systems using technoeconomic optimization and infrastructure planning methods. In our previous study, we developed a bottom-up design framework for a desert off-grid PVtH system integrated with water and hydrogen pipelines, showing the importance of dynamic water–power–hydrogen interactions and coordinated pipeline design [25]. Other recent studies have used HOMER-based optimization, plant-level sizing analysis, and regional comparison frameworks to optimize PV–electrolyzer configurations, storage, and hydrogen production economics [26–28], whereas recent reviews have summarized the dominant architectures and design variables of standalone and off-grid PV–H_2 systems [29–30]. Nevertheless, these modeling efforts remain largely disconnected, and a unified nonlinear multiscale framework for connecting PV temporal partitioning, water-mediated ecological interactions, and system-level cost, carbon, and biomass outcomes is still lacking.

Accordingly, the contributions of this study are threefold. First, this study proposes a new water–energy–ecology coupling mode by integrating PVtG and PVtH through segmented temporal partitioning (Fig. 1(a)), thereby enabling solar and water resources to jointly support both decarbonization and ecological restoration. Second, this study develops a nonlinear multiscale modeling framework that simulates PV operation and hydrogen production at a 5 km × 5 km spatial resolution, optimizes the infrastructure layout, and assesses the hourly impacts on energy and ecological systems across the Kubuqi Desert region in northern China. By linking module-scale PVtH conversion, network-scale infrastructure allocation, and system-level assessments of power, hydrogen, and ecological systems, the framework enables consistent evaluation of how local PV deployment decisions translate into system-wide decarbonization, financial cost, and biomass outcomes. Third, this study moves beyond fixed-scale feasibility analysis and reveals the sustainability pathway of segmented-profile PV expansion, including its scale effects, optimal strategy evolution, and breakpoint behavior. Our results show that integrating PVtH significantly reduces the total cost of achieving ecological and carbon-reduction targets compared with pure PVtG strategies; in particular, the optimal water–energy synergy strategy for utilizing 25.00 GW of PV generation reduces total costs by an average of 900 million USD relative to carbon capture and storage (CCS) and grass pads. Under suitable solar, water, land, and infrastructure conditions, this framework can be

extended to other arid regions globally, offering a scalable pathway to combine decarbonization with ecosystem restoration and informing segmented PPAs, targeted subsidies, and integrated water–energy policies.

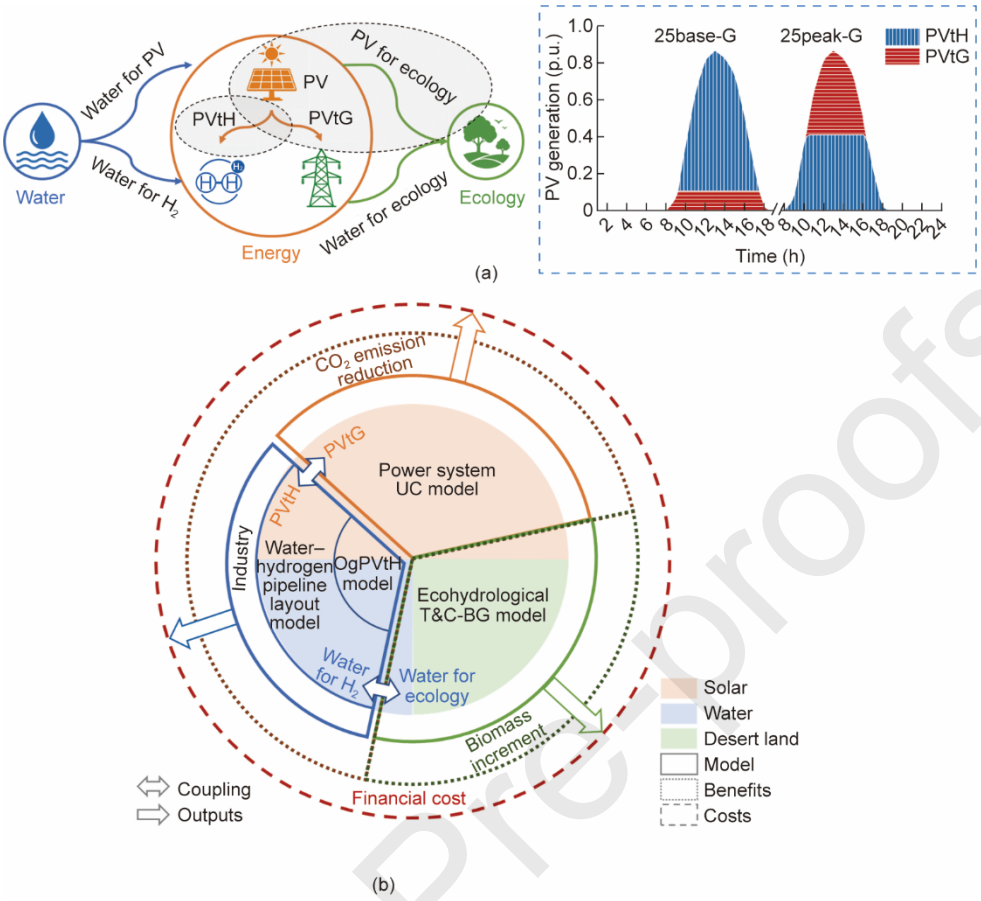


Fig. 1. Water–energy–ecology nexus, case-study deployment, and evaluation framework. (a) Conceptual illustration of the proposed nexus. Blue, orange, and green denote the water, energy, and ecology domains, respectively. PV output in the energy domain is partitioned between PVtG and PVtH, while water supports hydrogen production and ecological restoration. The gray shaded areas enclosed by dashed outlines indicate the scopes addressed by existing studies. The blue dashed inset illustrates temporal partition using the 25base-G and 25peak-G profiles; red and blue portions denote PVtG and PVtH generation, respectively, and the dashed boundary separates the base and peak segments. (b) Evaluation framework, described from the center outward. The orange, blue, and green filled sectors denote solar, water, and desert-land resources, respectively. Solid colored boundaries denote the model domains: orange for the power-system unit commitment (UC) model; blue for the hydrogen-system hierarchy, comprising the off-grid photovoltaic-to-hydrogen (OgPVtH) model at the module level, the water–hydrogen pipeline layout model at the network level, and hydrogen-industry assessment at the system level; and green for the Tethys–Chloris model with biogeochemistry (T&C-BG). Gray double-headed arrows denote the nonlinear PVtG–PVtH partition and water-for-hydrogen–water-for-ecology couplings. Outside the model domains, short dotted brown and green arcs denote CO_2 emissions reduction and biomass increment, respectively, whereas the outer long-dashed red boundary denotes financial cost. Colored outward arrows denote model outputs to the corresponding benefit and cost indicators.

2 Materials and methods

2.1 Case description

We evaluate how the deployment of desert PV panels to produce both grid power and green hydrogen can efficiently meet environmental goals.

Land. In Inner Mongolia, the Kubuqi Desert spans 14 100 km² and is primarily composed of fixed and semifixed sandy land with sparse vegetation (e.g., poplar, sand chrysanthemum, sand reed) [32].

Water. Water is sourced from the Yellow River [33], which supports both coal-based and electrolytic hydrogen production. In 2023, Inner Mongolia's total water supply from the Yellow River reached 10.40 billion tonnes, with 15% allocated to ecological purposes and 10% to industrial use. In this context, the optimal 25.00 GW PVtG–PVtH strategy in this study results in a decrease of 25.25 million tonnes (Mt) per year, which is substantially lower than the ~100 Mt per year currently required for regional coal-based hydrogen production [34], whereas PVtH itself requires only ~40 kg [35–36] of water per kg H_2. Water is assumed to be supplied from legally accessible Yellow River surface-water districts already serving industrial activities in the region rather than from additional groundwater abstraction.

Solar. The solar irradiance is ~1800 full-load PV hours annually on the basis of the ERA5-Land dataset [37–38] and is validated by local Kubuqi Photovoltaic Power Station data.

Electricity demand. The region is part of the West Inner Mongolia grid, with a total capacity exceeding 100 GW, of which 51.53 GW is fossil-based [39].

Hydrogen demand. The nearby Ordos base produces 2 Mt H_2 per year (6% of China's total) via coal gasification, emitting 24 Mt CO_2 [40].

2.2 Methods

2.2.1 Models

We develop a nonlinear multiscale evaluation framework to quantify CO_2 reduction, biomass increase, and financial costs under segmented-profile PV utilization, integrating high spatiotemporal resolution data (5 km × 5 km spatial resolution and 1 h temporal resolution), as shown in Fig. 1(b). At the model level, three interconnected domains are considered: a power-system model for the PVtG pathway (Section S3.1 in Appendix A), a hydrogen-system model for the PVtH pathway (Section S3.2 in Appendix A), and an ecohydrological model for the ecological pathway (Section S3.3 in Appendix A). The power system domain is represented by an 8760 h UC model for provincial grids and energy storage systems, which evaluates curtailment, thermal UC and ramping, coal consumption, operational costs, and CO_2 emissions under alternative PV partitioning strategies. The hydrogen system domain combines the off-grid PV-to-hydrogen (OgPVtH) optimization model and the water–hydrogen pipeline layout model, thereby linking module-scale water–power–hydrogen conversion with network-scale infrastructure allocation and allowing the evaluation of hydrogen production, fossil – hydrogen substitution, sectoral CO_2 emissions, and associated costs. The ecological domain is represented by the mechanistic Tethys–Chloris model with biogeochemistry (T&C-BG), which simulates hydrological processes, surface energy balance, carbon fluxes, and vegetation dynamics, with modifications to account for both PV shading and supplementary irrigation associated with panel cleaning and electrolyzer cooling.

These three model domains are linked through two nonlinear couplings. The first is the coupling of PV partitioning between PVtG and PVtH, by which the same PV output between grid export and hydrogen production simultaneously reshapes grid-side operation, hydrogen substitution, and water reuse. The second is the water-allocation coupling between water for hydrogen production and water for ecological enhancement, through which electrolysis, cooling and cleaning processes, supplementary irrigation, and ecological response are connected. Through these two couplings, local PV partitioning and water use decisions are propagated across scales and sectors so that the resulting system response is not a simple linear aggregation of the power, hydrogen, and ecological subsystems.

2.2.2 Indicators for benefits and costs

We define three key performance indicators—CO_2 emissions reduction, biomass increase, and financial costs—as the basis for scenario comparisons and strategy optimization, as shown in Fig. 1(b). The baseline for comparison is the state of the power system, hydrogen industry, and ecological systems in this region in 2025. The evaluation assumes that electricity and hydrogen demand levels remain constant across all scenarios, allowing the impact of different PV utilization strategies to be assessed independently.

CO_2 emission reduction. Carbon emissions are quantified from fossil fuel combustion in terms of both power generation and hydrogen production. Mitigation is achieved by replacing fossil fuel-based power and coal-based hydrogen production with PV generation and electrolytic green hydrogen. The metric is described in Section S2.2 in Appendix A.

Biomass increase. This indicator reflects the ecological benefit of quantifying the total increase in carbon stored in vegetation biomass and soil organic matter. Carbon dynamics are simulated through fluxes across multiple pools in response to environmental drivers—such as light, water availability, and temperature—modified by PV and hydrogen infrastructure. The metric is described in Section S2.3 in Appendix A.

Financial cost. The cost estimation includes both infrastructure-related fixed costs and system operation-related costs. Fixed costs include the annualized investment and operation costs of PV panels, transmission lines, substations, electrolyzers (EL), hydrogen storage (HS), water storage (WS), water pipelines (HP), and hydrogen pipelines (WP). The operating costs include coal consumption for power generation, additional coal consumption caused by thermal unit start-up and shut-down, and the avoided costs from replacing fossil-based electricity and hydrogen with PV electricity and green hydrogen. Specifically, desert PV deployment requires dedicated operation and maintenance (O&M), including fixed maintenance expenditures and regular panel cleaning, to mitigate dust-related soiling losses. In this study, PV O&M costs are explicitly represented by fixed O&M expenditures and the water cost of regular panel cleaning, while the corresponding cleaning-water input is incorporated into the water balance and ecohydrological assessment. The major technoeconomic assumptions used in the cost estimation are summarized in Table 1 [41 – 48]. All cost values in this paper are annualized for consistent comparison and evaluation; that is, upfront investment costs are converted to annual equivalents. A lower financial cost indicates a more economically competitive pathway, and a financial cost of zero means that the pathway no longer requires additional net financial support. The metric is described in detail in Section S2.1 in Appendix A.

Table 1.
Key technoeconomic assumptions used for cost estimation.

Parameter	Unit	Baseline value	Reference
Coal consumption for coal-based hydrogen production	kgce • kgH_2^{-1}	8.9	[41]
Coal consumption for coal-fired power generation	kgce • $(MW • h)^{-1}$	314	[42]
Electricity consumption for electrolytic hydrogen production	kW • h • kgH_2^{-1}	55	[43]
Coal price	USD • • kg^{-1}	0.11	[44]
PV capital cost	USD • kW^{-1}	428	[45]
Emission factor of coal consumption in power generation	$kgCO_2$ • $kgce^{-1}$	2.85	[46]
Emission factor of coal-based hydrogen production	$kgCO_2$ • kgH_2^{-1}	20	[41]
CCS cost for power sector	USD • • kg CO_2^{-1}	0.04	[47]
CCS cost for coal-based hydrogen sector	USD • $kgCO_2^{-1}$	0.03	[41]
Grass pad cost	USD • • m^{-2} • a^{-1}	0.14	[48]

kgce denotes kilogram of coal equivalent.

2.2.3 Scenarios

To explore viable pathways for decarbonization and ecological value in desert regions, we compare three strategies. The CCS + Grass Pads strategy serves as a benchmark to compare the costs of achieving environmental targets using PV strategies. The other two strategies are grid-only utilization (PVtG) and hybrid grid use with H_2 production (PVtG–PVtH). Their comparative performance across CO_2 reduction, biomass carbon increase, and financial cost is assessed for different scales of PV deployment.

CCS + Grass Pads. This strategy addresses decarbonization and ecological restoration separately. CCS reduces CO_2 emissions from fossil fuel-based power generation and hydrogen production. Grass pads are vegetative layers designed to stabilize soil and prevent erosion for desert restoration. The financial costs of this strategy include investment in grass pads and CCS infrastructure.

PVtG. This strategy reduces CO_2 emissions by replacing conventional fossil fuel-based power generation with clean PV generation. While PV panels do not directly influence biomass, they increase local microclimate factors, indirectly impacting biomass growth. The financial costs include the fixed cost of the PVtG infrastructure (including the investment and operating costs of PV panels and transmission lines) and the operating costs of the power system, which include the fuel and regulation costs. PVtG serves as the baseline solar strategy.

PVtG–PVtH. Building on PVtG, this strategy further eliminates CO_2 from conventional coal-based hydrogen production by using green electrolytic hydrogen. In terms of biomass, in addition to the indirect effects of PV, additional drip irrigation systems are implemented to reuse water for panel cleaning and electrolyzer cooling. Financial costs for this strategy account for the fixed cost of PVtH infrastructure in comparison with the current operating cost of hydrogen production, which includes expenses for feedstock and fuel (primarily coal).

To operationalize the PV-based strategies, we develop partitioning schemes that allocate PV generation between PVtG and PVtH across both spatial and temporal dimensions. Spatially, we simulate total PV deployment capacities ranging from 0 to 25.00 GW, in increments of 6.25 GW. Temporally, daily PV output is divided into base and peak segments, where the base period (blue in the lower right panel of Fig. 1(a)) corresponds to more stable generation and the peak period (red) corresponds to greater variability. Eight temporal allocation portfolios are constructed based on segmenting the total daily PV generation into base and peak periods and then allocating 0, 25%, 50%, 75%, or 100% of the base or peak daily output to grid use. The labels of the eight portfolios are shown on the strategy axes of Fig. 2; “25base-G” refers to a strategy where 25% of the daily output is considered the base generation and allocated to PVtG, while the remaining is regarded as peak generation and allocated to PVtH. Each portfolio label has two elements: the number indicates the percentage of the total daily PV generation, and the suffixes “base-G” or “peak-G” specify whether PVtG receives the base or peak generation. The two extreme cases—100% PVtG and 100% PVtH—are labeled simply as PVtG and PVtH, respectively, and represent full single-path utilization scenarios.

Journal Pre-proofs

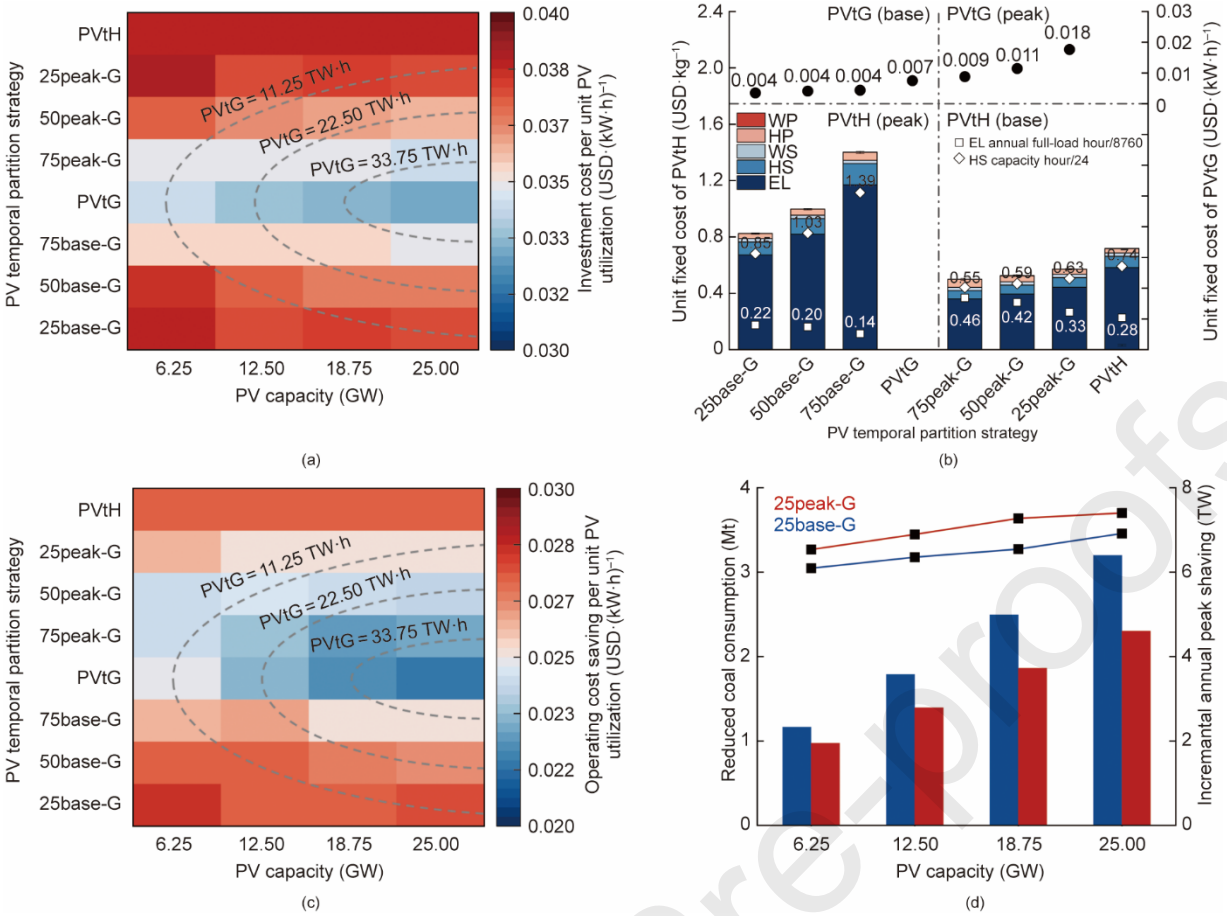


Fig. 2. Financial cost components and power-system effects across PV capacities and temporal partition strategies. (a) Unit fixed cost across combinations of PV capacity and temporal partition strategy. The color scale ranges from blue (lower cost) to red (higher cost), and gray dashed contours denote equal annual PVtG electricity delivery (11.25, 22.50, and 33.75 TW • h). (b) Unit fixed costs of PVtH and PVtG, excluding the PV capital cost shared by both pathways. Stacked bars on the left axis decompose PVtH cost into EL, HS, WS, HP, and WP. White squares and diamonds denote EL annual full-load hours divided by 8760 h and HS capacity hours divided by 24 h, respectively. Black circles on the right axis denote the PVtG unit fixed cost. The vertical dash-dotted divider separates strategies in which PVtG receives base and peak PV segments. (c) Unit operating cost savings across the same capacity–strategy combinations; the color scale and equal-PVtG contours follow panel (a). (d) Reduction in coal consumption (bars, left axis) and incremental annual peak shaving (lines with square markers, right axis) under the 25base-G (blue) and 25peak-G (red) strategies.

3 Results

3.1 Financial cost of water–energy infrastructure

3.1.1 Analysis of the fixed cost laws

We analyze unit fixed cost, defined as the (annualized) fixed cost of the PVtG and PVtH infrastructure per kilowatt hour of PV utilization. As shown in Fig. 2(a), for a given strategy, the unit fixed cost decreases as a function of PV capacity expansion. For a given PV capacity, when the PV utilization strategy transitions from 25base-G to PVtG over the first set of 4 strategies, the unit cost decreases with a higher share of PVtG. When the strategy moves from 75peak-G to PVtH, the unit cost increases with a lower share of PVtG. The contour lines represent the combinations of capacity and strategy that give a particular total TWh to the grid, providing a reference for evaluating cost trends.

To better understand the cost structure, we separate the fixed costs into PVtG and PVtH components (Fig. 2(b)), excluding the cost of PV panels shared by both. The fixed cost of PVtG includes substation expansion and transmission lines (unit cost 0.35–1.76 US cents per kilowatt-hour (cents • (kW • h)$^{-1}$)). As the strategy shifts from 25base-G to 25peak-G, the fixed costs of PVtG increase because of lower equipment utilization. For PVtH, the fixed cost covers the infrastructure for EL, WS and HS tanks, and WP and HP networks. The PVtH unit fixed cost ranges from 0.5 to 1.4 USD • kg^{-1} of hydrogen (0.86–2.57 cents • (kW • h)$^{-1}$). Under the 75peak-G strategy, with PVtH consuming the base 25% of PV generation, the levelized cost is the lowest (46% EL utilization and 13.2 h of storage). In contrast, under 75base-G, where PVtH consumes the peak 25%, the cost is the highest because of a sharp decrease to 14% EL utilization and storage needs expanding to 33.36 hours. Overall, compared with the base-G strategies, supplying the grid with PV peak generation (peak-G strategies) results in lower unit fixed costs.

3.1.2 Analysis of the operating cost laws

We define unit operating cost savings as the reduction in operating costs in power systems and hydrogen downstream industries per unit of PV energy generated. The operating cost savings for the strategy – capacity space are shown in Fig. 2(c) in the same manner as Fig. 2(a); the contour lines again represent a given level of terawatt hour delivered to the grid. For a given strategy, unit operating cost savings decrease monotonically with increasing capacity. For a given terawatt hour supplied to the grid, when the strategy transitions from 25base-G to PVtG (the first 4 strategies on the y-axis), and then from 75peak-G to PVtH, the unit operating cost savings decrease first and then increase along the contour line.

With respect to the pure PVtH strategy, the unit operating cost savings are driven by the replacement of coal-based hydrogen, reaching approximately 2.71 cents • (kW • h)$^{-1}$. For the hybrid strategies combining PVtG and PVtH, the unit operating cost savings range from 2.14 to 2.86 cents • (kW • h)$^{-1}$ depending on the share of PV allocated to the grid and differences in fuel and regulation costs in the power system. We evaluate power system impacts further in terms of coal consumption and peak-shaving requirements. Fig. 2(d) shows that 25base-G surpasses 25peak-G in terms of reduced coal consumption and lower incremental peak shaving. Meeting peak power demand when PV energy is insufficient requires additional coal consumption because of the more frequent on/off switching of thermal units. This results in an estimated extra coal consumption of 0.19 to 0.90 Mt. Additionally, energy storage systems are required to ramp up and down to further balance power, which leads to an additional 0.44 to 0.73 TW of peak shaving. These impacts contribute to higher overall operating cost savings for 25base-G.

Overall, allocating base generation to PVtG provides a more cost-effective utilization path under the partitioning strategy, balancing infrastructure investment and operational savings.

3.2 CO_2 reduction and biomass increase benefits

3.2.1 Analysis of the CO_2 reduction laws

The CO_2 reduction factor is defined as the net reduction in CO_2 emissions (from power and industry systems) per unit of new PV generation (kgCO_2 • (kW • h)$^{-1}$). The CO_2 reduction associated with the eight temporal strategies is shown in Fig. 3(a). For a given strategy, the CO_2 reduction factor decreases monotonically with increasing PV capacity. For a given increase in PV capacity, the CO_2 reduction factor increases monotonically with the PVtG ratio (from 25base-G to PVtG; from PVtH to 75peak-G), and the reduction factor increases as PVtG supplies base generation.

In Fig. 3(a), the average CO_2 reduction factor for the pure PVtH strategy is only 0.28 kg • (kW • h)$^{-1}$ across the four PV capacity additions studied. This net change includes an increase in the CO_2 emission factor of 0.08 kg • (kW • h)$^{-1}$ from newly deployed hydrogen infrastructure. For the other seven strategies that combine PVtG with PVtH, the CO_2 reduction factor ranges between 0.35 and 0.70 kg • (kW • h)$^{-1}$. This variation is primarily due to the structure of existing local power generation systems. The changes in the various sources of annual power generation (compared with the no-PV expansion base case) at two PVtG levels (11.25 and 45 TW • h) across the three strategies: 25base-G, PVtG, and 25peak-G are shown in Fig. 3(b). The results indicate a large increase in PV generation and a slight increase in wind generation, offsetting part of the reduction in coal-fired generation in the power sector. Power systems follow the economic dispatch rule, and some curtailed PV generation occurs. Thus, effective PV utilization is related to both PV capacity and the strategy for its use. As PV capacity expands, PV curtailment rates increase for all strategies, but the magnitude of the increase varies significantly. Specifically, at a PVtG output of 11.25 TW • h, the PV curtailment rates increase from 2% (25base-G) to 24% (25peak-G). When the PVtG source increases to 45 TW • h, these curtailment rates increase to 14% for 25base-G, and 47% for 25peak-G. For a given PVtG level, the curtailment rate for the 25base-G strategy is the lowest, whereas that for the 25peak-G strategy is higher because of the greater volatility in its generation profile. Although all three strategies result in higher curtailment rates with increasing PV capacity, the curtailment rate for 25base-G increases by only 14%, whereas that for 25peak-G increases by 23%, with a transition from the smallest addition to the greatest. This difference in PV curtailment rates directly affects the generation from coal-fired plants, which ultimately impacts the CO_2 reduction factor for PV utilization.

3.2.2 Analysis of the biomass increase

Beyond CO_2 emission mitigation, the ecological benefits of PV deployment are assessed through the analysis of increases in biomass. We evaluate the effects of different strategies by quantifying the biomass per unit area (gC • m^{-2}). As shown in Fig. 3(c), the average biomass in the natural recovery scenario is 52 gC • m^{-2}. The addition of PV panels results in a substantial increase of 79 gC • m^{-2}. Irrigation in the range of 30–43 mm further increases biomass by only 3 gC • m^{-2}.

The increase in biomass due to the use of PV panels can be attributed to two key factors, as illustrated in Fig. 3(d). First, the construction of PV panels increases surface roughness, resulting in a reduction in the wind speed from 2.10 m • s^{-1} under natural conditions to 1.66 m • s^{-1} in the PV scenarios. This creates a more stable wind field within the PV station, providing windbreak and sand-fixation effects that are beneficial for vegetation rooting and growth in desert regions. Consequently, vegetation coverage significantly increases from 0.1 under natural conditions to 0.5 in the PV scenarios. Additionally, the reduction in wind speed and net radiation decreases potential evaporation, increasing the soil moisture content from 0.035 to 0.044 with PV panels and to 0.046 with extra irrigation, further promoting vegetation growth.

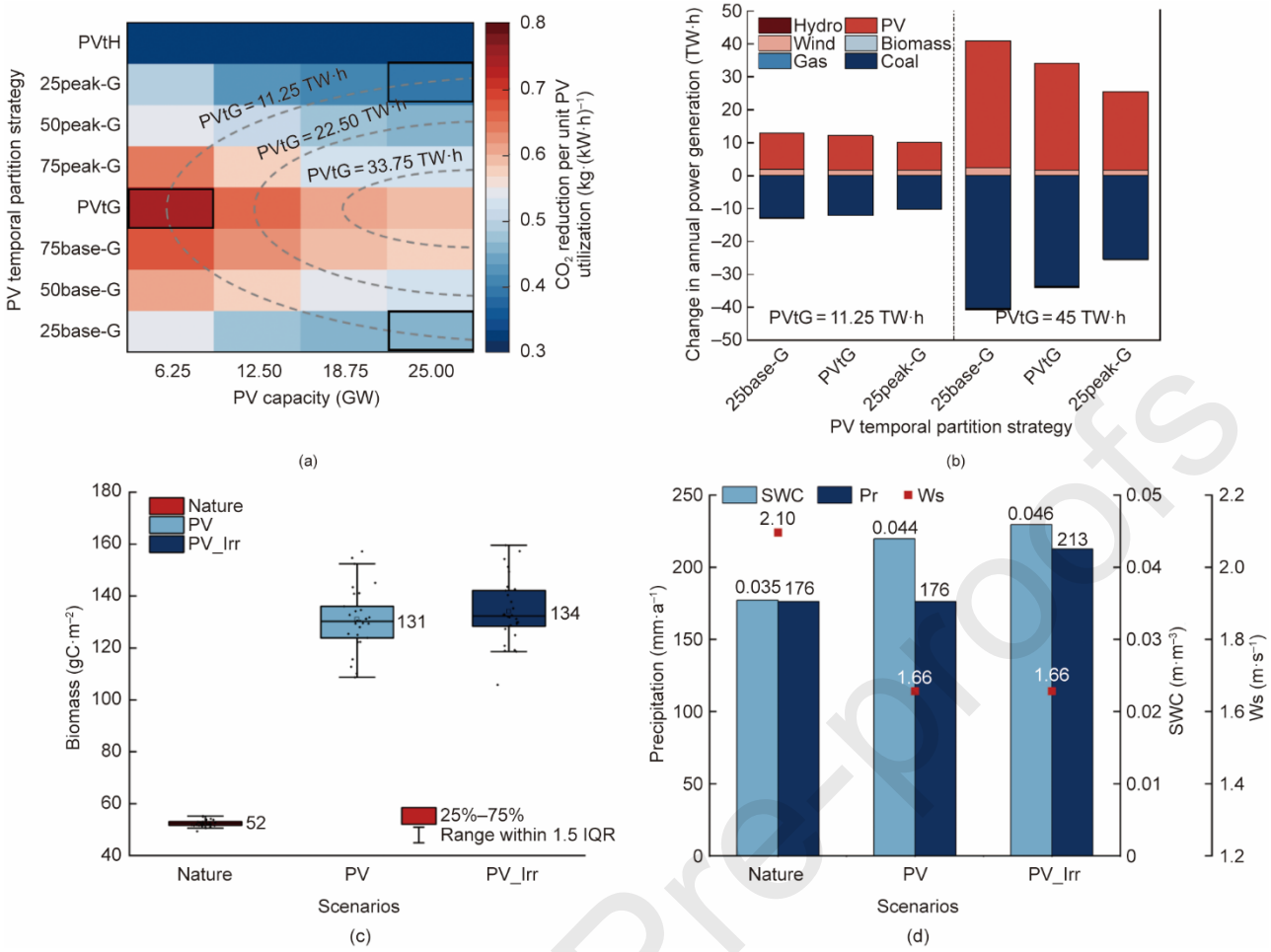


Fig. 3. CO_2 reduction and biomass responses across PV capacities and temporal partition strategies. (a) CO_2 emissions reduction per unit of PV utilization. The color scale ranges from blue (lower reduction) to red (higher reduction), and gray dashed contours denote equal annual PVtG electricity delivery. Black boxes identify the 25base-G, PVtG, and 25peak-G cases that each deliver 11.25 TW • h to the grid. (b) Changes in annual generation by source under PVtG deliveries of 11.25 and 45 TW • h for the 25base-G, PVtG, and 25peak-G strategies, respectively. Stacked colors denote coal, gas, biomass, hydropower, wind, and PV generation, respectively. (c) Annual biomass carbon density under natural recovery (Nature), PV panels without supplementary irrigation (PV), and PV panels with supplementary irrigation (PV_Irr). Dots denote annual values from the 30-year simulation (1987–2016); boxes show the 25th–75th percentiles and median, and whiskers extend to 1.5 times the interquartile range. (d) Mean growing-season soil water content (SWC; light-blue bars and inner right axis), annual precipitation (Pr; dark-blue bars and left axis), and mean wind speed (Ws; red squares and outer right axis) for Nature, PV, and PV_Irr. Growing-season SWC is averaged from May to October over 1987–2016. IQR: Interquartile Range.

3.3 Evolution of the optimal PV utilization strategy with PV capacity expansion

3.3.1 Analysis of cost scaling laws

We evaluate the total unit cost, defined as the sum of fixed and operating expenses, across different PV utilization strategies and PV deployment scales. The results are presented in Fig. 4(a) (with diamonds indicating different capacity additions). For the pure PVtG approach, the unit cost ranges from 0.95 to 1.11 cents • (kW • h)$^{-1}$, corresponding to an expansion from 6.25 to 25.00 GW. PVtG has an economic advantage at small scales but experiences diseconomies of scale as capacity expands to 25.00 GW, causing the unit cost to increase by 0.16 cents • (kW • h)$^{-1}$ and the total annualized financial cost to reach 0.50 billion USD at 25.00 GW. With respect to the pure PVtH approach, the unit cost varies narrowly, approximately 1.13 cents • (kW • h)$^{-1}$, with minor scale economies, and the total annualized financial cost is 0.51 billion USD. In the base-G strategy group, where PVtG primarily utilizes stable base generation, and PVtH absorbs peak generation, the unit cost is effectively reduced to the 0.93–1.06 cents • (kW • h)$^{-1}$ range. In contrast, for the peak-G strategy group, where PVtH uses base generation, and PVtG receives peak generation, the unit cost increases to the 1.07–1.31 cents • (kW • h)$^{-1}$ range. Along the optimal cost trajectory in Fig. 4(b), the preferred PV utilization strategy transitions sequentially from 75base-G (0–12.5 GW), to 50base-G (12.50–18.75 GW), and finally to 25base-G (18.75–25.00 GW). The PVtH share increases from 20% to 43.75% as the PV capacity expands to 25.00 GW. Compared with a fixed-strategy trajectory that follows 75base-G across all deployment scales, the scale-adaptive optimal trajectory reduces the total annualized financial cost from 0.46 to 0.45 billion USD.

3.3.2 Overall benefits and costs of the optimal PV utilization trajectory

The trajectories of CO_2 reduction and biomass increase along the optimal (least-cost) trajectory are shown in Fig. 4(b). At the largest scale of new PV considered (25.00 GW), the optimal trajectory will reduce CO_2 by 24 Mt (left axis) and increase biomass carbon by 40 kt (right axis) annually. The total annual water withdrawal reaches approximately 25 Mt (left axis). Considering that the unit PV investment cost ranges between 285 and 570 USD • kW^{-1}, with the default baseline set at 428 USD • kW^{-1} in the above discussion, the total annualized financial cost for deploying and utilizing 25.00 GW of PV generation along the optimal trajectory ranges from 0.06 to 0.82 billion USD, as shown in Fig. 4(c) (blue area). This corresponds to a unit CO_2 reduction cost of 3–34 USD • tCO_2^{-1}, excluding the additional economic value contributed by biomass. Compared with alternative options—deploying CCS [49] at both power and hydrogen downstream industries for CO_2 reduction and using grass pads [50] for desert restoration (pink area)—the proposed strategy achieves an average total cost reduction of 0.90 billion USD for 25.00 GW PV deployment (shown along the right *y*-axis of Fig. 4(c)).

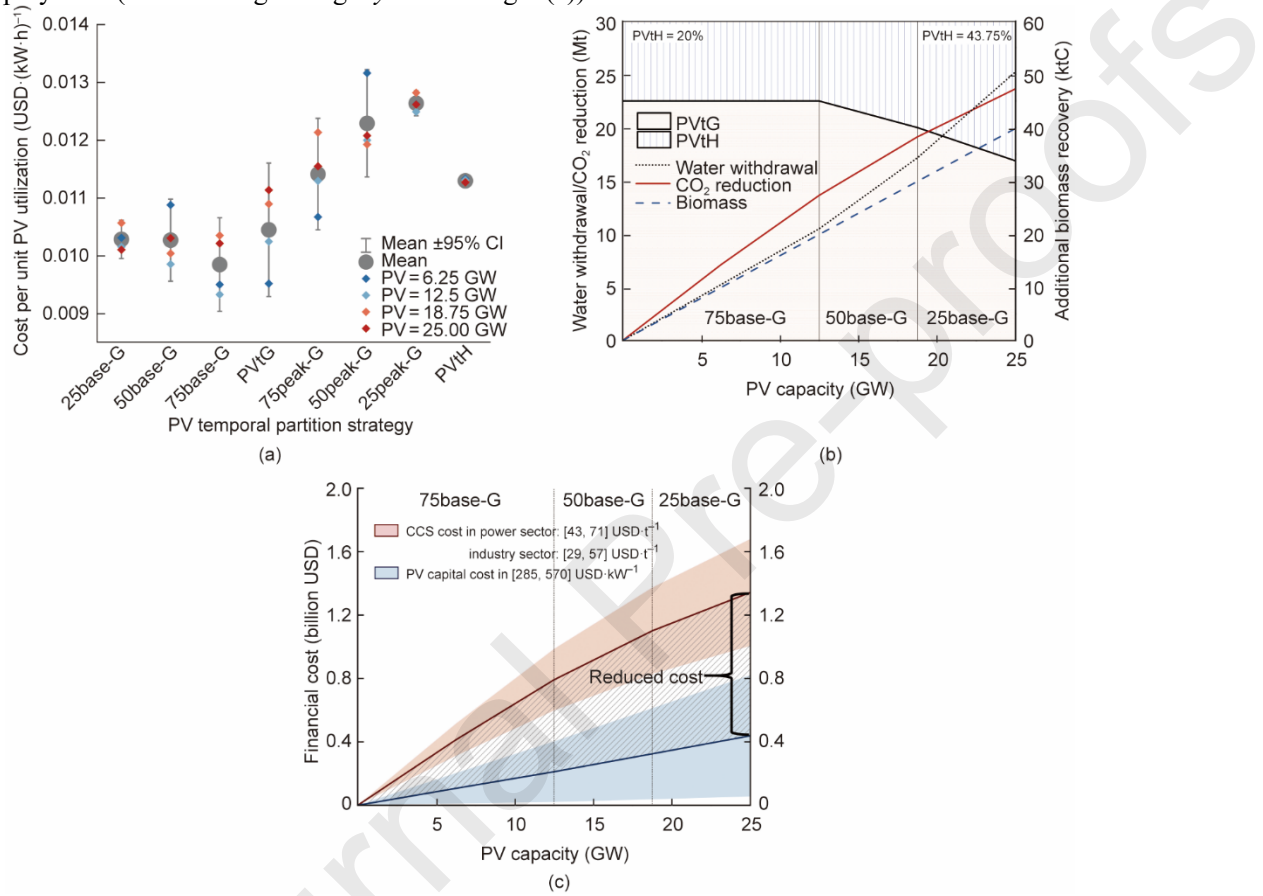


Fig. 4. Cost-efficient PV utilization trajectory and comparison with alternative mitigation and restoration measures. (a) Unit financial cost across PV capacities and temporal partition strategies. Colored diamonds denote the four PV-capacity additions (6.25, 12.5, 18.75, and 25.00 GW); gray circles and error bars denote the mean and 95% confidence interval for each strategy. (b) Water withdrawal (black dotted line, left axis), CO_2 emissions reduction (red solid line, left axis), and biomass carbon increment (blue dashed line, right axis) along the least-cost trajectory from 75base-G to 50base-G and then to 25base-G. White and vertically hatched regions denote the PVtG and PVtH shares, respectively, separated by the black trajectory boundary. (c) Cumulative financial cost of the least-cost PVtG–PVtH trajectory (blue range and mean line) compared with CCS and grass pads (red range and mean line). The PV capital-cost range is 285–570 USD • kW^{-1}. CCS costs are 43–71 USD • tCO_2^{-1} for power generation and 29–57 USD • tCO_2^{-1} for coal-based hydrogen production; the grass-pad cost is fixed at 0.14 USD • m^{-2} • a^{-1}. The bracket at 25.00 GW denotes the cost reduction achieved by the PVtG–PVtH trajectory relative to the benchmark. CI: Confidence Interval.

4 Discussion and conclusions

4.1 Sensitivity analysis of the optimal strategy

To examine the robustness of the optimal PV temporal partition strategy, six key parameters are analyzed in two groups. The first group includes internal system parameters, namely, electrolyzer efficiency, water availability, and energy storage capacity, which affect the physical feasibility and operational flexibility of the PVtG–PVtH pathway. The second group includes external economic and policy parameters, namely, PV capital cost, coal price, and carbon price, which affect the economic boundary conditions and transition breakpoints of large-scale PV deployment.

4.1.1 Internal system parameters: trajectory robustness and cost deviation

For the internal system parameters, the electrolyzer efficiency is varied by ±10%, the available water supply is reduced by 20% and 40%, and the energy storage capacity is increased by 100% and 200% relative to the benchmark 3 GW per 6 GW • h capacity. Under each perturbed case, the PV temporal partition strategy is reoptimized across PV capacities from 0 to 25.00 GW. These reoptimized trajectories are compared with the baseline optimal trajectory in Fig. 5(a). The left axis shows the discrete temporal partition strategy, while the right-axis markers quantify the deviation in the levelized cost of carbon reduction (LCOC), defined as the financial cost per unit of CO_2 emissions reduction. Specifically, the LCOC deviation is calculated as the LCOC obtained by retaining the baseline trajectory minus that obtained by reoptimizing the trajectory under the same perturbed condition. Thus, a deviation closer to zero indicates stronger robustness of the baseline pathway, whereas the sign indicates whether retaining the baseline trajectory yields a higher or lower LCOC than reoptimization does.

As shown in Fig. 5(a), the three internal parameters change this trajectory in different directions. When the electrolyzer efficiency increases by 10%, PVtH becomes more attractive, and the optimal strategy moves directly to 25base-G across the expansion range, indicating earlier and stronger hydrogen-side utilization. In contrast, when the electrolyzer efficiency decreases by 10%, the optimal pathway shifts toward more PVtG-oriented utilization, remaining at PVtG or 75base-G rather than transitioning to higher PVtH shares. This shift reflects the reduced conversion value of allocating PV electricity to hydrogen production. Water availability has the opposite effect. When the available water is reduced by 20%, the trajectory still shifts from 75base-G to 50base-G, but the transition to 25base-G is no longer selected at the largest PV scale. When the water availability is further reduced by 40%, the optimal trajectory remains at 75base-G throughout the expansion range. This finding indicates that water scarcity limits the feasible scale of PVtH and prevents the system from allocating a relatively large share of peak PV generation to hydrogen production. Storage expansion pulls the trajectory toward the grid side. When the storage capacity increases by 100%, the optimal strategy remains at approximately 75base-G, whereas a 200% increase in storage capacity shifts the pathway further toward PVtG-dominated utilization. This shift occurs because additional storage improves the power system's ability to absorb PV generation, thereby reducing the need to use PVtH as an alternative pathway for peak solar output. Overall, electrolyzer efficiency and water availability mainly determine whether PVtH can be expanded earlier and more deeply, whereas storage capacity determines whether grid-side flexibility can substitute for PVtH. Higher electrolyzer efficiency drives the trajectory toward more PVtH-oriented strategies, whereas lower water availability and greater storage capacity pull the trajectory back toward PVtG-oriented utilization.

With respect to electrolyzer efficiency, the LCOC deviation remains moderate, reaching approximately 0.10–2.24 USD • tCO_2^{-1} at 25.00 GW under a ±10% perturbation. The only negative deviation appears under the +10% efficiency case at small PV scales. This deviation occurs because higher efficiency makes PVtH more attractive in the reoptimized pathway, but the resulting larger PVtH share can reduce grid-side coal displacement. Therefore, the baseline pathway may yield a lower LCOC even with a higher absolute cost. Water availability produces the largest and most scale-sensitive deviation. In the −40% water case, the LCOC deviation is close to zero at 6.25–12.50 GW, increases to 18.75 GW, and reaches 9.18 USD • tCO_2^{-1} at 25.00 GW. This finding indicates that water becomes binding only when PVtH expands to a large scale. Storage capacity has the smallest LCOC deviation, remaining at approximately 1.05–1.12 USD • tCO_2^{-1} at 25.00 GW, although it visibly shifts the optimal strategy toward PVtG. This finding suggests that storage expansion changes the preferred allocation path more than it weakens the carbon-cost performance of the baseline pathway. Overall, the baseline trajectory is most robust to storage expansion, moderately sensitive to electrolyzer efficiency, and least robust to water availability. Water scarcity is therefore the key constraint for large-scale PVtH expansion.

Journal Pre-proofs

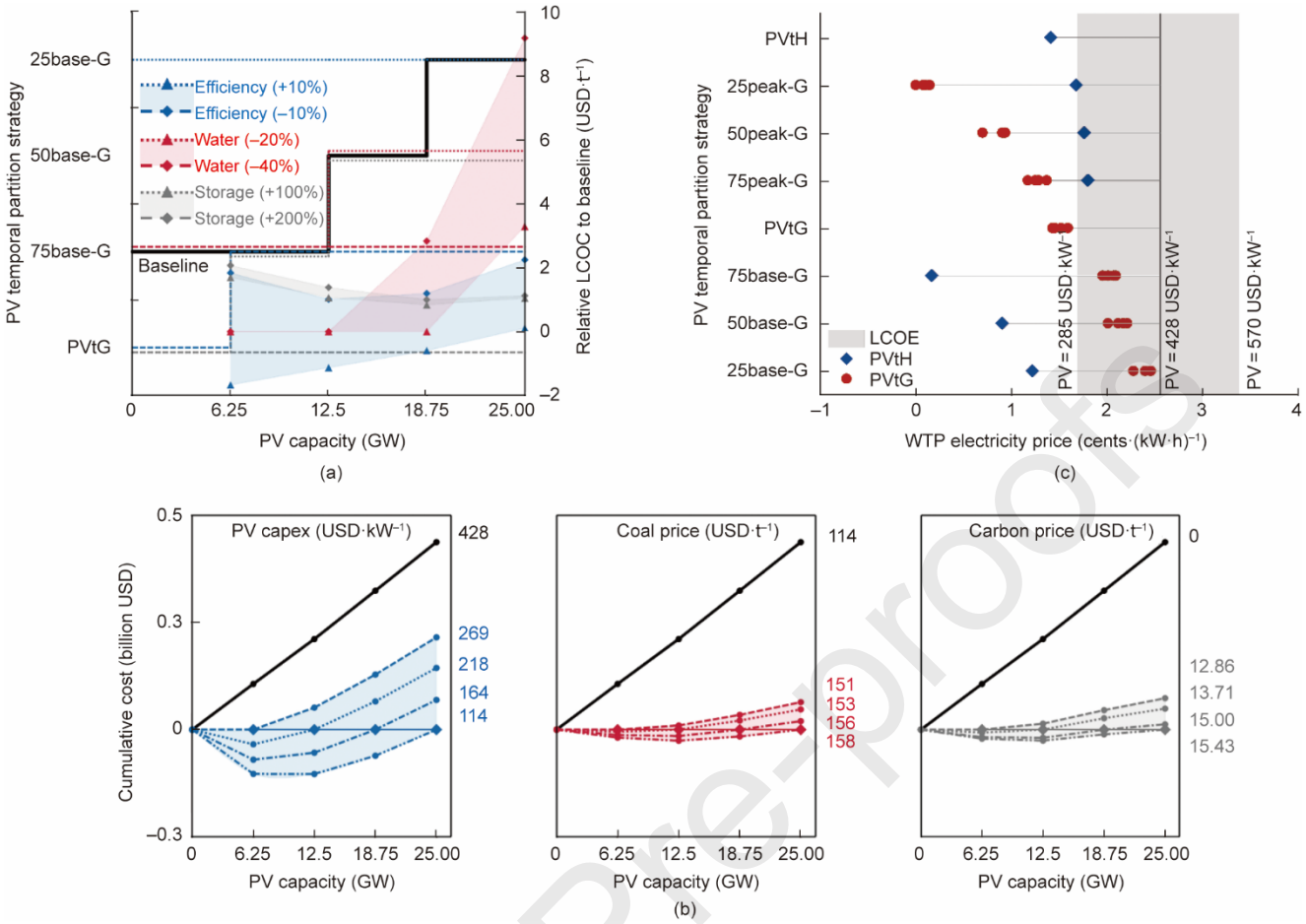


Fig. 5. Sensitivity and breakpoint analyses of the segmented-profile PV expansion pathway. (a) Re-optimized PV temporal partition trajectories and deviations in the levelized cost of carbon reduction (LCOC) under changes in internal system parameters. The black step line denotes the baseline trajectory. Blue, red, and gray step lines denote trajectories under changes in electrolyzer efficiency (±10%), water availability (−20% and −40%), and storage capacity (+100% and +200%), respectively; line styles and triangle or diamond markers distinguish the two cases for each parameter. Right-axis markers show the change in LCOC relative to the baseline value at the same PV capacity; positive and negative values indicate higher and lower LCOC, respectively. Shaded bands span the two perturbed cases for each parameter. (b) Breakpoint-implied cumulative financial cost trajectories for PV capital expenditure (capex), coal price, and carbon price. In each subpanel, the black line denotes the baseline trajectory, colored lines denote trajectories reconstructed at the four capacity-specific breakpoint values, and the shaded envelope spans these trajectories. Diamonds on the zero-cost line mark the capacities at which cumulative financial cost reaches zero; numbers on the right report the corresponding breakpoint values. Baseline parameter values are shown in black. (c) Stakeholder willingness-to-pay (WTP) for PV electricity and the levelized cost of electricity (LCOE). Red circles and blue diamonds denote the WTP of PVtG and PVtH stakeholders, respectively, across capacities and temporal partition strategies. The gray band denotes the PV LCOE range, and the vertical lines indicate assumed PV capex values of 285, 428, and 570 USD • kW^{-1}.

4.1.2 External economic and policy parameters: cost robustness and breakpoint analysis

With respect to the external economic and policy parameters, PV capital cost, coal price, and carbon price are analyzed through breakpoint-implied cumulative cost trajectories, with baseline values of 428 USD • kW^{-1}, 114 USD • t^{-1}, and 0 USD • tCO_2^{-1}, respectively. For each external parameter, breakpoint values are identified at the PV capacities of 6.25, 12.50, 18.75, and 25.00 GW, where the cumulative financial cost reaches the zero-cost boundary. Using these breakpoint values, Fig. 5(b) reconstructs the cumulative financial cost trajectories. The shaded envelopes show the range of cumulative costs induced by the breakpoint values of each parameter.

As shown in Fig. 5(b), the baseline cumulative financial cost increases monotonically with PV capacity and reaches approximately 0.45 billion USD at 25.00 GW, indicating that large-scale deployment still requires additional economic support under the benchmark assumptions. The three external parameters reduce this cumulative cost through different channels. PV capex has the strongest direct effect because it changes the investment base of all PV-based strategies. As the PV capacity expands from 6.25 to 25.00 GW, the zero-cost breakpoint of the PV capex decreases from 269 to 114 USD • kW^{-1}, corresponding to a reduction of approximately 37% to 73% relative to the baseline value of 428 USD • kW^{-1}. This declining breakpoint indicates that larger PV deployment requires increasingly lower investment costs to fully offset the cumulative financial burden. Coal price affects the avoided cost of replacing coal-based power generation and coal-based hydrogen production. Its zero-cost breakpoint

increases slightly from 151 to 158 USD • • t^{-1} with expanding PV capacity, corresponding to an increase of approximately 32% to 39% relative to the baseline coal price of 114 USD • • t^{-1}. This result suggests that higher coal prices improve the economic competitiveness of PVtG – PVtH deployment, but the increase in the required coal price becomes slightly greater at higher PV capacities because marginal PV utilization faces stronger integration and conversion costs. Carbon prices provide a policy-based value for avoiding fossil CO_2 emissions. Because the baseline carbon price is zero, the breakpoint is interpreted as an absolute threshold rather than a relative change. The required carbon price increases from 12.86 to 15.43 USD • • tCO_2^{-1} as the PV capacity expands from 6.25 to 25.00 GW. This moderate upward trend indicates that carbon pricing can effectively close the financial gap, but larger PV deployment requires a higher carbon value to compensate for declining marginal returns and rising system-integration costs. Overall, the PV capex determines the investment-cost floor of the pathway, whereas coal and carbon prices determine the value of fossil-fuel substitution. With increasing PV capacity, all three breakpoints move in a direction that implies that stronger economic conditions are needed for zero-cost deployment: lower PV capex, higher coal price, or higher carbon price.

4.2 Policy insights and engineering deployment

4.2.1 Water and land regulation

Policy support is needed to translate the optimized PVtG–PVtH trajectory into practical deployment. The first requirement is the coordinated regulation of land and water use. Hybrid PVtG–PVtH projects should be permitted only where surface-water access is legally available within existing industrial or ecological water-use quotas and where additional groundwater abstraction can be avoided. Land use regulation should also distinguish areas suitable for PV construction, ecological restoration, water storage, hydrogen production, and pipeline corridors. Such integrated zoning would help ensure that PV deployment, hydrogen production, and ecological restoration are planned as a coupled water–energy–land system rather than as separate sectoral projects.

4.2.2 Segmented PPAs pricing and targeted subsidies

The preceding analysis adopts a top-down planning perspective. Practical deployment, however, requires incentive alignment among governments, grid utilities, and hydrogen producers. We therefore propose a segmented PPAs mechanism in which the government supports PV deployment for ecological restoration, while grid utilities and hydrogen producers purchase PV electricity according to differentiated temporal profiles.

To evaluate this mechanism, we estimate the willingness to pay (WTP) for PV electricity from grid and hydrogen stakeholders under different PV scales and partitioning strategies. The WTP represents the maximum electricity price each stakeholder can afford while keeping PVtG or PVtH costs comparable to those of fossil-based alternatives in the absence of carbon pricing. By comparing WTP with the current levelized cost of electricity (LCOE) for PV, we identify feasible pricing ranges for different PV segments.

The WTP of grid utilities ranges from 0.14 to 2.29 cents • $(kW • h)^{-1}$, whereas that of hydrogen producers ranges from 0.14 to 1.86 cents • $(kW • h)^{-1}$(Fig. 5(c)). Both stakeholders assign higher values to stable base generation, but their WTP ranges are not symmetric. This asymmetry supports a tiered PPAs design in which stable base generation is associated with a higher price, whereas lower-value peak generation is priced lower and can be directed to hydrogen production.

Targeted subsidies are needed when the WTP of a stakeholder is below the PV LCOE. Along the optimal trajectory from 75base-G to 50base-G and then to 25base-G, the required average subsidies are 0.14–0.42 cents • $(kW • h)^{-1}$ for grid use and 1.29–2.43 cents • $(kW • h)^{-1}$ for hydrogen production, assuming a mid-range PV capital cost of 428 USD • kW^{-1}. The total subsidy required for the 25.00 GW optimal trajectory is 0.45 billion USD, including 0.34 billion USD for hydrogen producers and 0.11 billion USD for grid utilities. These subsidies lower realized PPAs prices and help align financial incentives with carbon reduction and ecological restoration goals.

4.2.3 Engineering applicability

At the engineering level, transferring this framework to other desert regions requires five boundary conditions: a legally accessible nongroundwater water supply, land suitable for both PV construction and ecological restoration, sufficient solar resources, accessible grid infrastructure, and nearby hydrogen demand or transport infrastructure. Beyond these requirements, the ecological response remains an open and site-specific factor because the effects of PV infrastructure on wind speed, soil moisture, vegetation growth, and water balance depend strongly on local climate and ecosystem conditions. Therefore, applying the proposed framework should be understood as localized adaptation under these engineering boundary conditions rather than direct replication of the Kubuqi case.

4.2.4 Monitoring and safety requirements

Future engineering demonstrations should include measurement systems for validating hydrogen, carbon, and water balances.

Hydrogen production and purity should be monitored at electrolyzer outlets and storage interfaces using flow meters and gas analyzers. CO_2 emissions from baseline fossil-based systems should be quantified using plant-level fuel-consumption records and continuous emission monitoring systems. Water withdrawal, reuse, and loss should also be recorded to verify the assumed water balance.

Hydrogen safety is another prerequisite for deployment. PVtH systems should include leak detection, ventilation, explosion-proof equipment, emergency shutdown systems, and appropriate separation distances around electrolyzers, storage tanks, and pipeline interfaces. Detailed hazard analysis and quantitative risk assessment are beyond the scope of this planning study but should be included in future pilot and commercial designs.

5. Conclusions

This study establishes a nonlinear multiscale framework for evaluating water–energy–ecology coupling in desert PV development. The Kubuqi case reveals a clear scaling pattern in terms of PV utilization. The cost-efficient trajectory shifts from 75base-G to 50base-G and then to 25base-G, increasing the role of PVtH as PV deployment expands. At 25.00 GW, this pathway delivers 25.30 TW • h of electricity, produces 0.36 Mt of green hydrogen, reduces CO_2 emissions by 24 Mt, and increases biomass carbon by 40 kt, with total cost savings of 0.90 billion USD compared with the CCS and grass-pad benchmarks.

The sensitivity analysis shows that the optimal PVtG–PVtH pathway is adaptive rather than fixed. Storage expansion has the strongest effect on the optimal trajectory, shifting the strategy back toward PVtG by improving the grid-side flexibility and reducing the need for hydrogen as a peak-PV outlet. Water availability is the most scale-sensitive constraint for PVtH expansion, with the LCOC deviation rising sharply at large PV capacities under severe water reduction. Electrolyzer efficiency affects mainly the conversion value of PVtH, while PV capital cost and coal price reshape the economic boundary of large-scale deployment by changing the investment floor and fossil-fuel substitution value. These findings suggest that future desert PV planning should move beyond single-sector capacity expansion toward integrated water, land, power, hydrogen, and ecological governance, supported by segmented PPAs, targeted incentives, and region-specific resource regulation.

One main limitation of this study is that the base–peak partition is derived from medium- to long-term planning profiles rather than being dynamically corrected with short-term PV forecast errors or market fluctuations. Future work could develop a rolling correction mechanism for the partition threshold, allowing the PVtG–PVtH allocation to be updated with improved forecasts while remaining within the feasibility region defined by the installed PV, grid, electrolyzer, storage, water, and hydrogen infrastructure. Further extensions could incorporate electricity market mechanisms and heterogeneous substitution costs across downstream sectors, such as chemicals, steel, and transportation. This approach would support the design of staged pathways, where green electricity and hydrogen are first directed to high-value or high-emission substitution opportunities and then gradually expanded to broader industrial and energy applications.

Journal Pre-proofs

CRediT authorship contribution statement

Jiarong Li: Conceptualization, Data curation, Software, Visualization, Formal analysis, Writing–original draft. **Zifu Zhang:** Data curation, Software, Visualization, Formal analysis, Writing–original draft. **Jiaxin Xu:** Data curation, Software, Writing–review & editing. **Jin Lin:** Conceptualization, Validation, Writing–review & editing. **Huimin Lei:** Conceptualization, Validation, Writing–review & editing. **Mun S. Ho:** Supervision, Writing–review & editing. **Chris P. Nielsen:** Supervision, Writing–review & editing. **Jianxiao Wang:** Software, Writing–review & editing. **Feng Song:** Supervision, Writing–review & editing. **Xinxin Pang:** Software, Writing–review & editing. **Yonghua Song:** Supervision, Writing–review & editing. **Michael B. McElroy:** Funding acquisition, Writing–review & editing.

Declaration of competing interests

The authors declare that they have no known competing financial interests or personal relationships that could have appeared to influence the work reported in this paper.

Acknowledgments

This research was supported by the National Natural Science Foundation of China (U23B20124), the Energy Foundation China (G-2209-34096 and G-2311-35278), and the Climate Imperative Foundation (2024-001465).

References

[1] Xing Q. Intranational synergies and trade-offs reveal common and differentiated priorities of sustainable development goals in China. Nat Commun 2024;15:2251.
[2] Haegel NM, Margolis R, Buonassisi T, Feldman D, Froitzheim A, Garabedian R, et al. Terawatt-scale photovoltaics: trajectories and challenges. Science 2017;356:141–3.
[3] Grodsky SM, Hernandez RR. Reduced ecosystem services of desert plants from ground-mounted solar energy development. Nat Sustain 2020;3:1036–43.
[4] Li Y, Kalnay E, Motesharrei S, Rivas J, Kucharski F, Kirk-Davidoff D, et al. Climate model shows large-scale wind and solar farms in the Sahara increase rain and vegetation. Science 2018;361:1019–22.
[5] Zhang N. The impact of photovoltaic power plants on surface energy budget based on an ecohydrological model. Renew Energy 2023;212:589–600.
[6] Li Z, Jiang Y, Yang L, Jiang Y, Luo Y, Gao X. A comparative study on the surface radiation characteristics of photovoltaic power plant in the Gobi desert. Renew Energy 2022;182:764–71.
[7] Wu C, Liu H, Zhao W, Song S, Li L, Yin L, et al. Ecohydrological effects of photovoltaic solar farms on soil microclimates and moisture regimes in arid Northwest China: a modeling study. Sci Total Environ 2022;802:149946.
[8] Jiang J, Broadbent AM, Krayenhoff ES, Georgescu M. Observed impacts of utility-scale photovoltaic plant on local air temperature and energy partitioning in the barren areas. Renew Energy 2021;174:157–69.
[9] Hernandez RR, Armstrong A, Burney J, Ryan G, Moore-O'Leary K, Heath GA, et al. Techno-ecological synergies of solar energy for global sustainability. Nat Sustain 2019;2:560–8.
[10] Yu S, Fu S, Behrendt J, Chai Q, Chen L, Chen W, et al. Synthesis report 2022 on China's carbon neutrality: electrification in China's carbon neutrality pathways. Report. Beijing: Energy Foundation China; 2022. Chinese.
[11] Bhambhani A. World's 'largest' wind & solar PV project coming up in China [Internet]. Dusseldorf: TaiyangNews; [cited 2026 Apr 26]. Available from: https://taiyangnews.info/markets/worlds-largest-wind-solar-pv-project-coming-up-in-china/.
[12] Li J, Du E, Zhang N, Zhang Y, Zhang B, Kang C, et al. Coordinated planning of HVDCs and power-to-hydrogen supply chains for interregional renewable energy utilization. IEEE Trans Sustain Energy 2022;13:1913–29.
[13] Miao B, Giordano L, Chan SH. Long-distance renewable hydrogen transmission via cables and pipelines. Int J Hydrogen Energy 2021;46:18699–718.
[14] Hausfather Z. Quantifying solar value deflation in California [Internet]. Berkeley: The Breakthrough Institute; [cited 2026 Apr 26]. Available from: https://thebreakthrough.org/articles/quantifying-solar-value-deflation.
[15] Yang X, Nielsen CP, Song S, McElroy MB. Breaking the hard-to-abate bottleneck in China's path to carbon neutrality with clean hydrogen. Nat Energy 2022;7:955–65.
[16] Yan J. Negative-emissions hydrogen energy. Nat Clim Chang 2020;8:560–3.
[17] International Energy Agency. An energy sector roadmap to carbon neutrality in China [Internet]. Paris: International Energy Agency; [cited 2026 Apr 26]. Available from: https://www.iea.org/reports/an-energy-sector-roadmap-to-carbon-neutrality-in-china.
[18] Peng M, Zhao Y, Li J, Jing Z. Collaborative planning of hydrogen refuelling stations and DRGs in ADN for distributed energy consumption and flexibility enhancement. Appl Energy 2025;396:126253.
[19] Gabrielli P, Aboutalebi R, Sansavini G. Mitigating financial risk of corporate power purchase agreements via portfolio optimization. Energy Econ 2022;109:105980.
[20] Trabesinger W, Kanellakopoulou M, Bavin D. Baseload PPAs: essential tips for developers and lenders [Internet]. Schlieren: Pexapark; [cited 2026 Apr 26]. Available from: https://pexapark.com/blog/deconstructing-baseload-ppas-essential-tips-for-developers-and-lenders/.
[21] Pinos J, Munson SM, Karban CC, Petrie MD. Ecovoltaic solar energy development creates novel microclimate, temperature, and soil moisture patterns

under solar panels in a warm desert. Ecol Process 2026;15:33.
[22] Yu Z, Zhang Z, Yuan R. Identifying the causal effects of photovoltaic installations on grassland productivity using double machine learning: a case study in Inner Mongolia. Sci Rep 2026;16:39023.
[23] Yang R, Zhou W, Chen S, Li W, Zhang T, Wang Y, et al. Photovoltaic deployment on suitable marginal land in China enables energy and sustainability co-benefits. Commun Earth Environ 2026;7:6555.
[24] Liu H, Wu C, Zhao W, Song S, Li L, Guo L, et al. Ecological and environmental effects of global photovoltaic power plants: a meta-analysis. J Environ Manage 2025;370:123506.
[25] Xu J, Lin J, Li J, Lin R, Pan G. Optimal design and techno-economic analysis of a desert off-grid photovoltaic-to-hydrogen system integrated with pipeline networks. Energy Convers Manage 2025;336:119864.
[26] Lebepe MC, Oviroh PO, Jen TC. Techno-economic optimization modeling of a solar-powered hydrogen production system for green hydrogen generation. Sustain Energy Res 2025;12:11.
[27] Rojas J, Garcia A, Martin J, Ruiz P, Sanchez M, Gomez J, et al. Integrated plant design for green hydrogen production and power generation in photovoltaic systems: balancing electrolyzer sizing and storage. Hydrogen 2025;6:7.
[28] Mena R, Ruiz J, Perez A, Lopez M, Garcia S, Martin P, et al. Techno-economic evaluation of solar-driven PEM water electrolysis systems for hydrogen production: comparison and regional insights. Renew Energy 2026;250:125558.
[29] Alzahrani A, Ali M, Khan A, Bakhsh F, Rehman S, Al-Shahrani S, et al. Assessment of standalone energy generation systems integrating photovoltaic arrays, electrolyzers, and fuel cells: a review. Int J Hydrogen Energy 2026;51:5446–78.
[30] Montoya-Acevedo D, Renaudineau H, González-Castaño C, Restrepo C, Kouro S, Crestana-Guardial E. Off-grid photovoltaic green hydrogen production systems: a review. Renew Sustain Energy Rev 2026;236:116972.
[32] Chen P, Wang S, Song S, Wang Y, Wang Y, Gao D, et al. Ecological restoration intensifies evapotranspiration in the Kubuqi Desert. Ecol Eng 2022;175:106504.
[33] Yellow River Conservancy Commission of the Ministry of Water Resources. Yellow River water resources bulletin 2023 [Internet]. Zhengzhou: Yellow River Conservancy Commission of the Ministry of Water Resources; [cited 2026 Apr 26]. Available from: http://www.yrcc.gov.cn/gzfw/szygb/202409/P020240929336008326942.pdf. Chinese.
[34] Xia Y, Shi J, Zhao Z, Liu Z, Liu X, Zhang C. Mapping the coal-water nexus in the Yellow River Basin. J Clean Prod 2023;411:137249.
[35] Lampert D, Cai H, Elgowainy A. Wells to wheels: water consumption for transportation fuels in the United States. Energy Environ Sci 2016;9:787.
[36] Blanco H. Hydrogen production in 2050: how much water will 74 EJ need? [Internet]. London: Energy Post; 2015 Jul 22 [cited 2026 Apr 26]. Available from: https://energypost.eu/hydrogen-production-in-2050-how-much-water-will-74ej-need/.
[37] Muñoz Sabater J. ERA5-Land hourly data from 1950 to present [dataset]. Manila: Copernicus Climate Change Service (C3S) Climate Data Store; 2019 Jul 12 [cited 2026 Apr 26]. Available from: https://cds.climate.copernicus.eu/datasets/reanalysis-era5-land?tab=overview.
[38] Lin H, Hernandez Gonzalez A, Nielsen CP, McElroy MB. Texas: a green hydrogen hub to decarbonize the United States and beyond. Proc Natl Acad Sci U S A 2024;121:e2321347121.
[39] Inner Mongolia Government. Installed capacity of the West Inner Mongolia power system reaches 100 GW [Internet]. Hohhot: Inner Mongolia Daily; 2024 Jan 01 [cited 2026 Apr 26]. Available from: https://www.nmg.gov.cn/zwyw/gzdt/bmdt/202401/t20240101_2434828.html. Chinese.
[40] National Energy Administration, Energy Conservation and Equipment Department, Beijing Guohydrogen Zhonglian Hydrogen Energy Technology Research Institute. China hydrogen development report 2023. Report. Beijing: People's Publishing House; 2023. Chinese.
[41] Wei YM, Liu L, Li X, Yan R. The carbon footprint and cost of coal-based hydrogen production with and without carbon capture and storage technology in China. J Clean Prod 2022;362:132514.
[42] National Energy Administration of the Peoples' Republic of China. Notice of the National Energy Administration on issuing the 2016 energy work guidelines [Internet]. Beijing: National Energy Administration of the People's Republic of China; 2016 Mar 22 [cited 2026 Apr 26]. Available from: https://zfxxgk.nea.gov.cn/auto82/201604/t20160401_2219.htm. Chinese.
[43] Standards Press of China. GB 32311-2015: minimum allowable values of energy efficiency and energy efficiency grades for hydrogen producing systems by water electrolysis. Chinese standard. Beijing: Standards Press of China; 2015. Chinese.
[44] National Development and Reform Commission of the People's Republic of China. Notice of the National Development and Reform Commission on further improving the mechanism for forming coal prices [Internet]. Beijing: Nation Development and Reform Commission of the People's Republic of China; 2022 Feb 22 [cited 2026 Apr 26]. Available from: https://www.ndrc.gov.cn/xxgk/zcfb/tz/202202/t20220225_1317003_ext.html. Chinese.
[45] Chen X, Liu Y, Wang Q, Lv J, Wen J, Chen X, et al. Pathway toward carbon-neutral electrical systems in China by mid-century with negative CO_2 abatement costs informed by high-resolution modeling. Joule 2021;5:2715–41.
[46] Peng W, Li Y. Application of gray relational analysis in evaluating the environmental loads in Hubei Province, China, during 1995–2019. Pol J Environ Stud 2024;33(3):2773–86.
[47] Chu B, Lin B, Tian L, Zheng C, Ye N, Zhu Y, et al. A long-term impact assessment of carbon capture (storage) investment conducted by conventional power company on sustainable development. Appl Energy 2024;358:122567.
[48] Zhong S, Han Z, Li A, Du H. Research on the application of palm mat geotextiles for sand fixation in the Hobq Desert. Sustainability 2019;11(6):1751.
[49] Global CCS Institute. CCS progress in China-a status report. Report. Melbourne: Global CCS Institute; 2023.
[50] Zhou Y, Li H, Wu Z, Wang Z, Yin J, Qing D, et al. Sand fixation mechanism and effect evaluation of sand barriers in Mu Us sandy land, China. Chin Sci Bull 2023;68:1312–29. Chinese.

(i) A water–energy–ecology nexus is proposed for desert PV development.

(ii) PV generation is partitioned between grid electricity and green hydrogen.

(iii) A nonlinear multi-scale framework links module, network, and system levels.

(iv) Hybrid PVtG–PVtH reduces system costs by up to 0.10 cents/kWh.

(v) Scaling PVtH improves sustainability as grid-side PV value declines.

Declaration of Interest Statement

☒ The authors declare that they have no known competing financial interests or personal relationships that could have appeared to influence the work reported in this paper.

☐ The author is an Editorial Board Member/Editor-in-Chief/Associate Editor/Guest Editor for this journal and was not involved in the editorial review or the decision to publish this article.

☐ The authors declare the following financial interests/personal relationships which may be considered as potential competing interests:

Jiarong Li

Journal Pre-proofs